



Potential causes of megadroughts in North China in the preindustrial period from the teleconnection perspective

Xuezhen Zhang^{a,b}, Mengxin Bai^{a,b,c}, Zhixin Hao^{a,b}, Jingyun Zheng^{a,b,*}

^a Key Laboratory of Land Surface Pattern and Simulation, Institute of Geographic Sciences and Natural Resources Research, Chinese Academy of Sciences, Beijing 100101, China

^b University of Chinese Academy of Sciences, Beijing 100049, China

^c Faculty of Geographical Science, Beijing Normal University, Beijing 100875, China

ARTICLE INFO

Editor: Trude Storelvmo

Keywords:

North China
External forcing
Teleconnection
Megadrought
Atmospheric circulation anomaly

ABSTRACT

The potential causes of megadroughts over North China (NC) in the preindustrial period were investigated using eight climate models evolved using CMIP5/PMIP3 and multiple proxy data. The full forcing experiments driven by both external forcing and internal variability show that megadroughts in NC were accompanied by extensive decadal drying over the Northern Hemisphere (NH), particularly in most of North America and Europe. The spatial pattern of hydroclimate matched well with the proxy-based illustration. However, such hydroclimate conditions over NH were difficult to reproduce in control experiments driven solely by internal variability. This finding suggests that external forcing may be a crucial factor leading to megadroughts in NC and simultaneous decadal drying over the NH. Moreover, external forcing may lead to climate cooling. Climate cooling weakened the pressure gradient from the West Pacific to East Asia and hence reduced the water vapor to land; meanwhile, local vertical downward movement occurred in the cooling climate background, which was unfavorable to air convection over NC. Both reduced water vapor and weakened air convection led to less precipitation. Meanwhile, there was a negative NAO, which intensified the eastward wave train at mid-latitudes. Consequently, the North American trough and European trough deepened, the northerlies in the post trough pattern intensified, and the water vapor from the high-latitude continent or polar areas was low, which was unfavorable to precipitation. This study implies that the megadrought in NC and simultaneous hydroclimatic spatial pattern over the NH may be underestimated in the CMIP5 climate prediction, which excludes external forcing.

1. Introduction

Drought is a major natural hazard that may reduce grain production, cause water resource deficits and lead to catastrophes for humans (Xie et al., 2014; Zarei et al., 2016). It is reported by Ministry of Water Resources of the People's Republic of China that grain losses in China caused by drought were reaching 39.2 billion kilograms per year from 1990 to 2008, which accounted for ~1.47% of GDP losses. North China (NC) is characterized by a large population density and high grain production, and it is one of the regions vulnerable to drought in China (Jiang et al., 2017; Wang et al., 2018). Moreover, due to high variability of East Asia summer monsoon (EASM), NC is frequently suffering from drought. Due to human-induced global warming in the 21st century, the drought risks would increase (Chen et al., 2018; Yuan et al., 2019).

Therefore, drought is a hot topic in the climate science community.

Megadrought is a prolonged severe drought with decadal scale in comparison to general drought (Cook et al., 2016). Due to its catastrophic effects, it has been extensively studied. Yu et al. (2014) reported that the megadrought areas over NC increased by almost 2.89% per decade during the past five decades. Wang et al. (2011) reported that more frequent and extended duration of megadrought has likely occurred since the 1990s. Instrumental meteorological measurements in China mostly started in the mid-20th century. As a consequence, megadroughts retrieved from instrumental measurement data are very limited, and our knowledge on megadroughts is thereby limited as well.

To overcome the limitations of instrumental measurement data, hydroclimate (i.e., drought/flood and precipitation) variations over the past several hundred years and millennia were reconstructed using

* Corresponding author at: Key Laboratory of Land Surface Pattern and Simulation, Institute of Geographic Sciences and Natural Resources Research, Chinese Academy of Sciences, Beijing 100101, China.

E-mail address: zhengjy@igsrr.ac.cn (J. Zheng).

<https://doi.org/10.1016/j.gloplacha.2021.103596>

Received 31 January 2021; Received in revised form 24 June 2021; Accepted 30 July 2021

Available online 11 August 2021

0921-8181/© 2021 Elsevier B.V. All rights reserved.

climatic proxy data (i.e., tree ring and historical documents) (Zheng et al., 2006; Cook et al., 2010; Shi et al., 2017). It shows that there have been lots of serious megadroughts in the 10th, 14th, and 15th centuries in NC since 500 CE, and they were all much more serious than anyone in the instrumental measurement period (Zheng et al., 2006; Ge et al., 2013; Ning et al., 2019), with the largest extents in the 1580s, 1630s, and 1870s (Shi et al., 2017). These proxy-based findings suggest that there have been more megadroughts in NC in the pre-instrumental period. Therefore, in the context of climate change during the last millennium, additional megadrought samples would be available and, thereby, to overcome limitations of instrumental measurements data to improve our understanding of the characteristics and mechanisms of megadroughts.

A large number of studies have contributed to understand causes of megadrought in NC. Some studies reported that external forcing, such as volcanic eruptions and solar irradiation minimum, may be dominant causes. The volcanic eruptions may lead to surface cooling (Driscoll et al., 2012; Timmreck, 2012) and, hence, to intertropical convergence zone (ITCZ) shift equatorward (Stevenson et al., 2016) as well as the El Niño mode over the tropical central-east Pacific Ocean (Ohba et al., 2013; Sun et al., 2019) or strengthened western Pacific subtropical high (Shen et al., 2007). Consequently, the EASM weakened and precipitation in the monsoon region (i.e., North China) decreased (Schneider et al., 2009; Stevenson et al., 2016). Solar irradiation minimum may alter the atmospheric energy budget and exert cooling effects on surface, which may weaken the land–ocean thermal contrast and hence decrease water vapor transport in East China (van Loon et al., 2007; Man et al., 2012).

Meanwhile, there are also a lot of studies highlighting importance of internal variability, such as air–sea interactions and atmospheric oscillations. It is reported that a positive phase of the Pacific Decadal Oscillation (PDO) (Yu et al., 2014; Yang et al., 2017; Zhou et al., 2020), positive phase of the Atlantic Multidecadal Oscillation (AMO) (Yang et al., 2019), or positive phase of the North Atlantic Oscillation (Peng, 2018) may trigger a mid-latitude zonal wave train and further enhance cyclones near the Korean Peninsula, which may ultimately weaken the EASM to East China and decrease precipitation in NC. Taken together existing studies, the causes of megadroughts in NC during the preindustrial period are complicated and, the dominant leading factor of megadrought is being remained unclear.

It is noted that abovementioned results were mostly obtained from regional evidences while little from continental and hemispherical evidences. It is well known that effects of external forcing are globally. The effects of internal variability, such as PDO, AMO, and AO, are also continental or hemispheric scale rather than being constrained only in NC and East Asia. Following atmospheric teleconnection theory, changes in meteorological elements between two remote areas could be closely linked with each other through atmospheric circulation. As a result, the regional climatology anomaly in the NC caused by external forcing or internal variability may be accompanied by climatology anomaly in other areas. The hydroclimate anomaly spatial pattern at continental and hemispheric scale would be valuable clue to understand potential cause of regional megadrought. This idea has been applied successfully by Coats et al. (2016), who studied the hydroclimate anomaly over the NH when megadrought occurred in western North America during the last millennium and found that it may be caused by internal variability. However, the supporting evidences from other area have not been paid attentions by existing study for the megadrought in NC.

Herein, this study aims to explore the potential cause of megadrought in NC during the last millennium from the perspective of teleconnection. This study addresses the following questions: (1) What is the spatial pattern of hydroclimate over the NH when megadrought occurred in NC during the preindustrial period? (2) What are the potential causes leading to megadrought in NC? The remainder of the paper is organized as follows. Section 2 introduces the data and approaches; Section 3 presents the results; Section 4 discusses the spatial

patterns of hydroclimate directly triggered by external forcing in proxy data and the probability of megadrought reoccurring during the RCP scenarios; and Section 5 presents the conclusions and potential research directions.

2. Data and approach

This study used both climate model simulation data and proxy data to depict historical climate changes. First, we quantitatively predefined megadrought events as a decadal drought with a frequency threshold of 5% during the last millennium. Following this criterion, we selected megadrought decades for NC from the climate modeling data and proxy data, respectively. Then, the simultaneous hydroclimate spatial patterns over the NH when megadroughts occurred in NC were depicted. Next, modeling datasets were used to explore the potential causes and mechanisms of megadrought in NC.

2.1. Simulation data

This study used climate modeling data, including both control experiments and full forcing experiments, which were derived from a total of eight climate models involved in the Coupled Model Intercomparison Project Phase 5 (CMIP5)/ Paleoclimate Modeling Intercomparison Project Phase 3 (PMIP3). The control experiments employ constant external forcing, including solar irradiation, greenhouse gases (e.g., CO₂, CH₄ and N₂O) (GHGs) and Land Use/Cover Change (LUCC), which were all maintained at the preindustrial level. As a result, control experiments represent climate changes driven solely by internal variability. The full forcing experiments employ real-time, dynamic external forcing consisting of volcanic aerosols, solar irradiation, GHGs, and LUCC (Taylor et al., 2012). Thereby, full forcing experiments represent climate changes driven together by both external forcing and internal variability.

It should be noted that precipitation anomalies over the 20th century have been largely related to anthropogenic factors (sulfate aerosols and greenhouse gases) (IPCC, 2013). Therefore, this study used only the last millennium (850–1850 CE) of climate modeling from the full forcing experiments rather than entire period from 850 to 2005 CE. Additionally, we also applied climate predictions under the RCP4.5 scenario and RCP8.5 scenario. Details of the models are summarized in Table 1, including the institutes and horizontal and vertical resolutions. Bothe et al. (2013) pointed out that MIROC-ESM modeling simulation results were inconsistent with other climate modeling results and may present opposite temperature situations with proxy data. Therefore, we only used eight climate models from CMIP5/PMIP3 in this study.

2.2. Proxy data

Two sets of proxy-based hydroclimate datasets were used. The first dataset is the regional decadal-resolved dry-wet index for the North China (approximately east of 105° E and 34–40° N) covering 500 to 2000 CE. This dataset was generated by calculating the dry and wet frequency within a smooth window of 10-year using the drought/flood

Table 1
CMIP5/PMIP3 models used in this study.

Model	Country	Atmosphere resolution	RCP4.5	RCP8.5
BCC-CSM1.1	China	~2.8° × ~2.8°, L17	√	√
CCSM4	USA	1.25° × ~0.9°, L17	√	√
CSIRO-Mk3L-1-2	Australia	~5.6° × ~3.3°, L18		
FGOALS-s2	China	~2.8° × ~1.7°, L17	√	√
GISS-E2-R	USA	2.5° × ~2.0°, L17	√	√
HadCM3	UK	3.75° × ~2.5°, L17		
IPSL-CM5A-LR	France	3.75° × ~1.9°, L17		
MPI-ESM-P	Germany	~1.9° × ~1.9°, L25		

√ denotes that the model provides outputs of the RCP4.5 and 8.5 scenarios.

grading retrieved from historical documentary records from the 21 stations in NC (Zheng et al., 2006). Moreover, a significant correlation ($r = 0.66$, $p < 0.05$) existed between NC dry-wet index and regional precipitation during 1870–2000, which indicates that the historical document-based dry-wet index could represent the historical precipitation variations. This dataset has been used extensively to analyze long-term hydroclimate variations in NC and the long-term evolution of the EASM (Zheng et al., 2006; Chen et al., 2010; Graham et al., 2011).

The second dataset is an annually resolved dry-wet proxy index serials from 196 sites over the NH, mostly spanning from 800 to 2000 CE (Ljungqvist et al., 2016). These sites are mostly distributed in the mid-high latitudes (30° N–70° N), including East Asia, Europe and the United States. The proxy data consists of lake sediments (81 serials, 41.33% of the total serials), tree rings (45 serials, 22.96%), speleothems (28 serials, 14.29%), peat cores (18 serials, 9.18%), documentaries (13 serials, 6.63%), ice cores (6 serials, 3.06%), and marine sediments (5 serials, 2.55%). Moreover, these serials were validated with GHCNS instrumental precipitation at the decadal time scale. The median correlation coefficient of all serials was 0.66 ($P < 0.05$), which indicates that the multi-proxies-based dry-wet index could represent the historical precipitation variations. In addition, the specific proxy data sources can be found in Ljungqvist et al. (2016). The dataset was extensively applied in hydroclimate studies of East Asia and Europe (Ljungqvist et al., 2019; Schneider et al., 2019).

2.3. Approach

2.3.1. Transform precipitation into SPI

Precipitation is known to follow a skewed distribution, with high (low) frequency in light (heavy) rain. The standardized precipitation index (SPI) is a widely used index conforming to a normal distribution to characterize meteorological drought and better quantify precipitation anomalies on multiple time scales. Therefore, following the method of McKee et al. (1993), we first fitted the monthly precipitation of each grid cell in full forcing experiments and control experiments. We assumed the monthly precipitation following the gamma distribution and defined the probability density function with Eq. (1).

$$g(x) = \frac{1}{\alpha^\beta \Gamma(\beta)} x^{\beta-1} e^{-x/\alpha} \quad (1)$$

where α is the scale parameter, β is the shape parameter, Γ is the gamma function, and x is the monthly precipitation in each grid cell.

$$\alpha = \frac{1}{4m} \left(1 + \sqrt{1 + \frac{4m}{3}} \right) \quad (2)$$

$$\beta = \frac{\bar{x}}{\alpha} \quad (3)$$

$$m = \ln(\bar{x}) - \frac{\sum \ln(x)}{k} \quad (4)$$

where k in full forcing experiments is 12,012 derived from 1001 years (from 850 to 1850 CE) multiplied by twelve months, k in the control experiments is the total number of years (inconsistent among models) multiplied by twelve months, and \bar{x} is the monthly precipitation climatology mean from 850 to 1850 CE.

Then, we calculated the cumulative probability function of precipitation based on $g(x)$ in Eq. (1).

$$G(x) = \int_0^x g(x) dx \quad (5)$$

Finally, we transformed the cumulative probability distribution into a standard normal distribution and yielded SPI with Eq. (6). We calculated the mean value of monthly SPI from Jan. to Dec. as the annual SPI.

$$SPI = \begin{cases} -\left(s - \frac{d_0 + d_1 p + d_2 p^2}{1 + e_1 p + e_2 p^2 + e_3 p^3} \right) & \text{for } 0 < G(x) \leq 0.5 \\ +\left(s - \frac{d_0 + d_1 p + d_2 p^2}{1 + e_1 p + e_2 p^2 + e_3 p^3} \right) & \text{for } 0.5 < G(x) < 1 \end{cases} \quad (6)$$

where $d_0 = 2.515517$; $d_1 = 0.802853$; $d_2 = 0.010328$; $e_1 = 1.432788$; $e_2 = 0.189269$; and $e_3 = 0.001308$.

$$p = \begin{cases} \sqrt{\ln\left(\frac{1}{(G(x))^2}\right)} & \text{for } 0 < G(x) \leq 0.5 \\ \sqrt{\ln\left(\frac{1}{(1-G(x))^2}\right)} & \text{for } 0.5 < G(x) < 1 \end{cases} \quad (7)$$

2.3.2. Selection of megadrought events in North China from climate modeling and proxy datasets

For the modeling data, we first calculated the NC regional mean SPI for each model. Then, decadal SPI serials were generated through smoothing with a window of 10-year. Next, following the frequency threshold of 5%, we selected the top five decadal drought events in NC from the decadal SPI during the past millennium for each model and 40 megadroughts were totally obtained from 8 models. To minimize the effects of uncertainties of individual climate models on the analysis results, we finally calculated the multi-model ensemble mean SPI and meteorological factor anomalies corresponding to the decadal drought events of NC.

To maintain comparability, the same parameters were employed in the transformation from precipitation to SPI for the past millennium climate modeling and for the RCP4.5 and RCP8.5 scenario climate projections. Meanwhile, the SPI threshold value for the megadrought event also remained unchanged in both the past millennium climate modeling and RCP4.5 and RCP8.5 scenario climate projections for each climate model. Therefore, the megadrought events from climate projections would be comparable to those from past millennium climate modeling.

For proxy data, following the frequency threshold of 5%, the top five decadal drought events were identified from the dry-wet index of Zheng et al. (2006). Meanwhile, to homogenize multiple proxy records indicating hydroclimate, Ljungqvist et al. (2016) first normalized the 196 serials over the NH. Then, based on normalized data, new annually resolved dry-wet index series were generated by linear interpolation. Finally, we calculated dry-wet proxy index for each site and, as a result, depicted the spatial pattern of hydroclimate over the NH during the top five megadrought events in NC.

3. Results

3.1. Simulated hydroclimate patterns over the NH

Because of the discrepancies among the climate models and the uncertainties of each model, the timing of the five most severe megadrought events varies from one climate model to another (figure not shown). Herein, we depict the ensemble mean SPI anomaly coexisting with the NC megadrought from all climate models (Fig. 1). We found that when megadrought occurred in NC, there were mainly extensive dry conditions with the exception of North Africa and western North America in the full forcing experiments, while zonal dryness and wetness belts coexisted in the control experiments over NH. In detail, the full forcing experiments of 850–1850 CE showed that dry conditions existed surrounding NC except in southern China. Meanwhile, dry conditions also existed in western and northern Europe, Greenland, the northern portion of North America, Northeast Asia, and low latitudes of Africa. Notably, significantly anomalous wet conditions existed in North Africa and the western United States. In total, the significantly

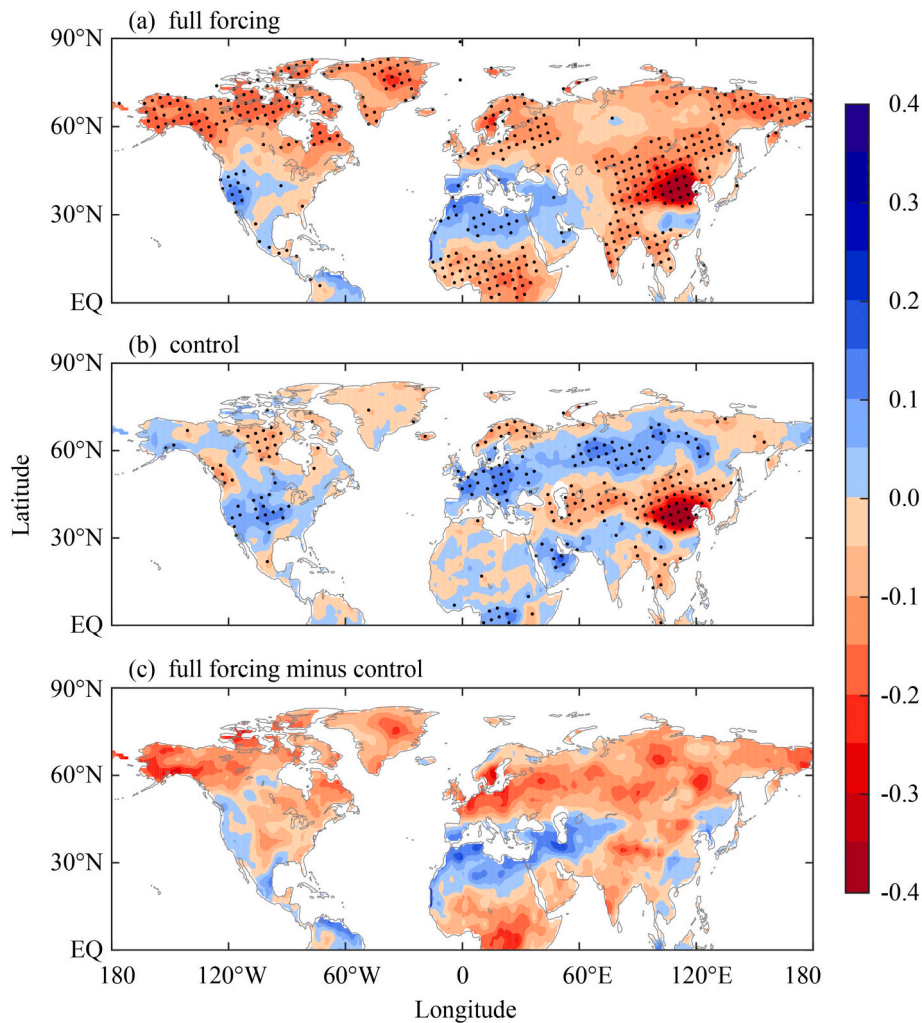


Fig. 1. Spatial pattern of the multi-model ensemble mean anomaly of SPI (relative to 850–1850 CE) through the five severest megadroughts over North China in the full forcing simulations (top), control simulations (middle) and their differences (bottom). The black dots denote significance at a confidence level of 0.05.

anomalous dry conditions accounted for approximately 40.59% of the Northern Hemisphere land area, while wet conditions only accounted for approximately 6.37%.

In the control experiments, dry conditions still existed around the NC but to a smaller extent than in the full forcing experiments. On the one hand, the significant dry conditions disappeared in South Asia; on the other hand, the northern edge of the significantly anomalous dry area moved southward. Meanwhile, significantly anomalous dry areas extend westward to Central Asia. Notably, a significantly anomalous wet belt existed from western Europe to Siberia in Russia, which was occupied by dry conditions in the full forcing experiments. Meanwhile, a significant anomalous wet conditions extends from the western coastline of the United States to the central area, and only a very small area of the northern partition of North America was occupied by significant anomalous dry conditions. Moreover, the hydroclimate in Africa also thoroughly reversed those from the full forcing experiments. The low latitudes of Africa were occupied by slightly wet conditions, and northern Africa was approximately neutral. In total, the significantly anomalous dry conditions accounted for approximately 15.60% of the Northern Hemisphere land area, while wet conditions only accounted for approximately 12.71%.

These findings illustrate that the hydroclimate spatial patterns over the Northern Hemisphere during megadrought in NC from the full forcing experiments differ from those obtained in the control experiments. The essential differences in settings between the full forcing

experiment and the control experiment are with or without dynamic external forcing. Therefore, these findings suggest that the hydroclimate over the NH when megadrought occurs due to only internal variability is different from those due to both external forcing and internal variability. Megadrought in NC based only on internal variability may be limited within the domain from northern China to central Asia; however, based on a combination with external forcing, megadrought in NC is accompanied by extensive decadal drying in the Northern Hemisphere, excluding North Africa and the western US.

3.2. Reconstructed hydroclimate patterns over the NH

Fig. 2a shows the five most severe megadroughts of NC in 1146–1155, 1240–1249, 1483–1492, 1578–1587, and 1634–1643 (Fig. 2a). The decadal mean dry-wet indices for these megadrought events ranged from -3.21 to -2.26 . Historical document records have indicated that these megadroughts cause great destruction to human society, such as by the synchronized relationship between these megadroughts and the poor harvests (Hao et al., 2020). From 1634 to 1643 CE, ~ 20 million people died from famine, and this severe megadrought was a key trigger for the peasantry uprising in the late Ming Dynasty (Zheng et al., 2014).

Fig. 2b shows the proxy data-based hydroclimate spatial patterns over the Northern Hemisphere. These proxy data refer to natural archives, such as tree rings, speleothems, lake sediment, pollen, etc.;

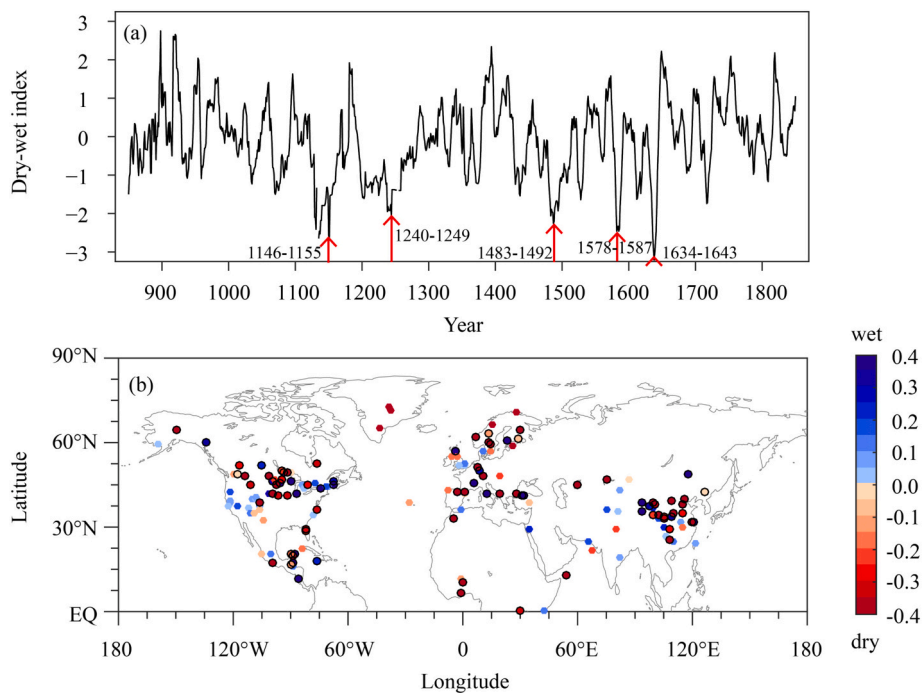


Fig. 2. Regional mean dry-wet index over NC in preindustrial periods (Zheng et al., 2006) (a), with red arrows representing the five severest megadroughts and the hydroclimate pattern over NH through the five severest megadroughts in NC (b). The black circles denote significance at a confidence level of 0.05. (For interpretation of the references to colour in this figure legend, the reader is referred to the web version of this article.)

hence, they are independent from the dry-wet index (Fig. 2a) derived from only historical document records. The natural archives illustrate that abnormal dry conditions with hydroclimate anomalies of approximately -0.3 prevail over NC. Such anomalous dry conditions are consistent with those derived from historical documents. Therefore, the hydroclimate indicated by historical documents and by natural archives could be verified with each other. It is notable that the proxy data in Central Asia mostly indicate wet conditions with only one exception. These wet conditions suggest that the megadroughts in NC have not extended to Central Asia. However, both the full forcing simulations and control simulations consistently suggest westward extension of drought from NC. Hence, neither the full forcing simulation nor the control simulation could reproduce the hydroclimate anomaly in central Asia when megadrought occurred in NC.

In Europe, there are many negative dry-wet indices with mosaics of positive values (Fig. 2b). In total, among the 40 proxy data serials, there are negative mean dry-wet indices in 25 serials. These negative indices suggest that dry conditions were predominant over Europe, with megadroughts occurring in NC during the last millennium. In particular, the negative indices accounted for more of the portion in northern Europe than in southern Europe. A comparison of Fig. 1 and Fig. 2b showed that hydroclimate from the full forcing experiments likely matches better with that from the proxy data because both of these data consistently present extensive dry anomaly conditions, while the reverse is true for the control experiments.

In North America, predominantly positive dry-wet indices suggest that wet conditions are observed in the western Contiguous United States (CoUS) and negative dry-wet indices suggest that dry conditions are observed in the central partition. The dry conditions indicated by the negative dry-wet index also likely prevailed over eastern North America but with some exceptions. Meanwhile, in Central America, there was also a likely predominant negative dry-wet index, suggesting dry conditions. Additionally, the three available serials over Greenland consistently exhibit negative indices, suggesting dry conditions. By comparison with Fig. 1, we find that full forcing experiments likely match better with the proxy data illustration because they reproduce these differences characterized by wet conditions in the western CoUS

and dry conditions in central to eastern North America as well as in Central America, while the control experiments present predominant wet conditions across North America.

For tropical Africa, the scarce availability of proxy data illustrates that there may be predominantly dry conditions (Fig. 2b). By comparing simulations, we found that the full forcing experiment reproduced the dry conditions in tropical Africa while control simulations illustrated wet conditions.

The abovementioned results show that neither full forcing simulations nor control simulations present the hydroclimate anomaly spatial pattern exactly the same as the proxy data illustration over the entire Northern Hemisphere. Clarifying the discrepancy between the simulations and proxy data illustrations is difficult since there are inherent uncertainties for any individual event. However, as mentioned above, the comparisons of simulations against the proxy data illustration show that the full forcing experiments reproduce the spatial pattern of hydroclimate anomalies well while control experiments do not. These findings suggest that megadroughts in NC and simultaneous hydroclimate anomalies over Europe, North America, and tropical Africa may not occur in the absence of external forcing. Thus, these megadroughts in NC and their simultaneous hydroclimate over the NH may be caused by external forcing and internal variability rather than solely by internal variability.

3.3. Atmospheric anomalies when megadrought occurred in the NC

Since full forcing experiments could reproduce megadroughts in NC and simultaneous decadal dry conditions in most of Europe and North America, full forcing experiments outputs were used by this study to depict atmospheric anomalies. Fig. 3a shows that a surface air cooling background generally occurred over the NH during megadrought events in NC. There were some severe cold centers with temperatures as low as -0.5 °C, such as over the northern United States and northeastern Europe. In comparison to continental cooling, cooling over the ocean, i. e., the Pacific and the Atlantic, was relatively weaker. In addition, the surface air temperature of NC experienced local warming of approximately 0.2 °C. Studies have proposed that severe summer drought in NC may reduce evapotranspiration and further decrease latent heat and

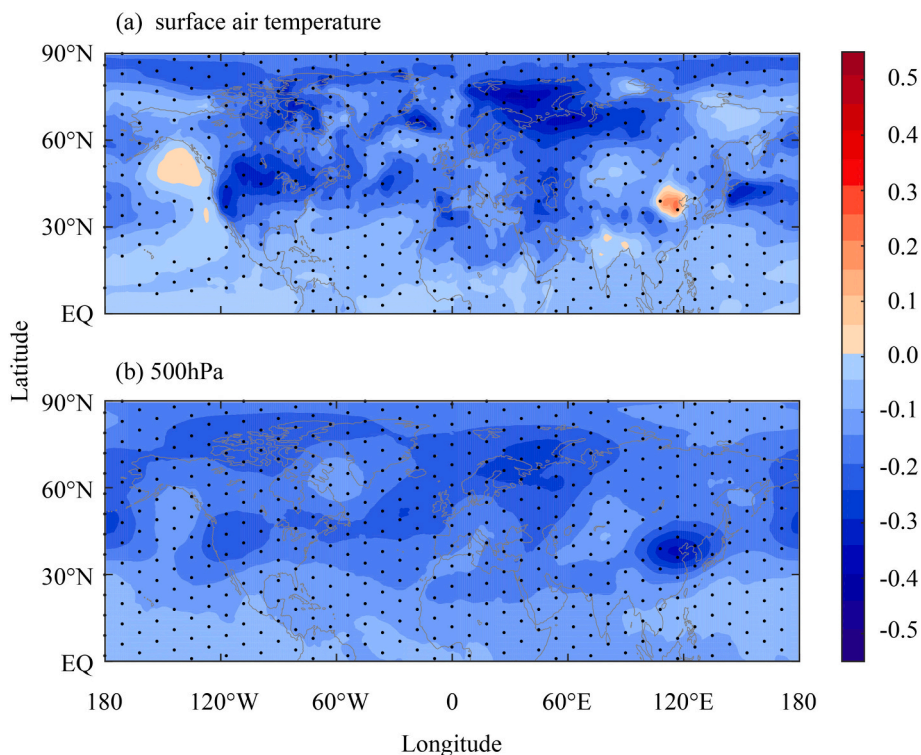


Fig. 3. Spatial pattern of the surface air temperature anomaly for the five megadroughts (a) and the temperature anomaly at the 500 hPa pressure level (b). The black dots denote significance at a confidence level of 0.05.

increase sensible heat. So, the local warming over NC may be derived from local feedback of land-air interactions (Stegehuis et al., 2013; Erlingis et al., 2019). Meanwhile, the local warming only existed at bottom of atmosphere within a limited area. This finding as well as supported that it is derived from feedback of land-air interactions rather than atmospheric circulations. Fig. 3b shows that the air temperature in the mid-troposphere entirely declined over the NH. These findings indicated that the integrated atmospheric column presented cooling affected by external forcing. It is noted that drought in other areas of NH land is weaker than NC megadrought (Fig. 1a) and, hence, warming derived from land-air interactions may neutralized external forcing-induced cooling. This may explain there is no warming at bottom of atmosphere over the drought area with an exception of NC.

Due to the different amplitude of surface air cooling between land and ocean, the weakened land-sea thermal contrast was further weakened. Hence, there would be an anomalous sea level pressure gradient from East Asia characterized by high anomalies to the West Pacific characterized by low anomalies (Fig. 4b) by referring to the climatology summer land-sea pressure gradient. We also noted a significant cyclone over the Sea of Japan whose western boundary was NC (Fig. 5a). Taken together, we find that intensified northerlies from boreal areas may partly offset the EASM and decrease water vapor transport (Fig. 5b), and as a consequence, these conditions are unfavorable to precipitation.

In another perspective, under the global cooling background affected by external forcing, the joint effects of cold advection (Fig. 3b) and a low-pressure trough (Fig. 4b) at the 500 hPa pressure level may largely reduce the thickness of the integrated column atmosphere over NC. Horizontal wind convergence occurred at the 500 hPa pressure level (Fig. 6a) and with vertical downward movement (Fig. 7). Thus, a local vertical downward movement may largely hinder lifting condensation of water vapor and hence is unfavorable for precipitation in NC. These results suggest that northerlies induced by horizontal circulation anomaly and downward movement over NC together decrease precipitation.

Meanwhile, Fig. 4a shows that the geopotential height of the 500 hPa pressure level entirely descended over the NH except north of 80°N in the

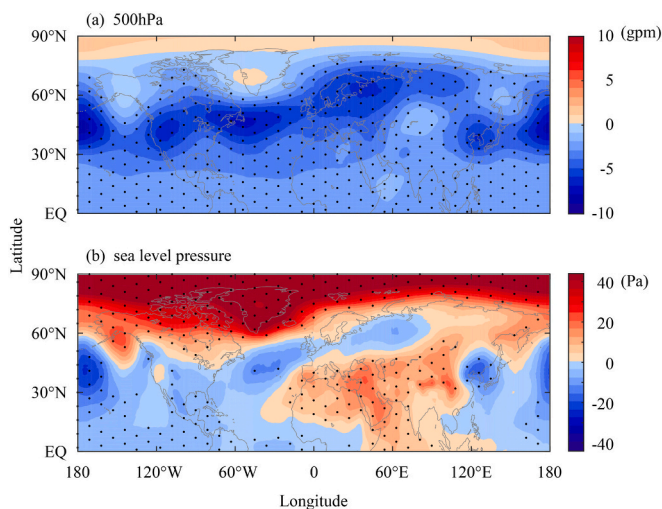


Fig. 4. Spatial pattern of the geopotential height anomaly of the 500 hPa pressure level for the five megadroughts (a) and sea level pressure anomaly (b). The black dots denote significance at a confidence level of 0.05.

context of external forcing. There were some anomalous low-pressure centers in the mid-latitudes, such as the middle of the Atlantic and eastern Europe, northeastern China and the North Pacific. Importantly, we found that a dipole pattern occurred over the Atlantic, which was consistent with the negative phases of the North Atlantic Oscillation (NAO) patterns and may generally be stimulated by external forcing (i.e., volcanic eruptions) (Henson et al., 2013). In addition, the eastward wave train in the mid-latitudes stimulated by the negative NAO strengthened the meridional disturbance of Rossby waves and, as a result, formed several anomalous low-pressure centers, such as over the eastern Europe, northeastern China and eastern North America. The locations of these

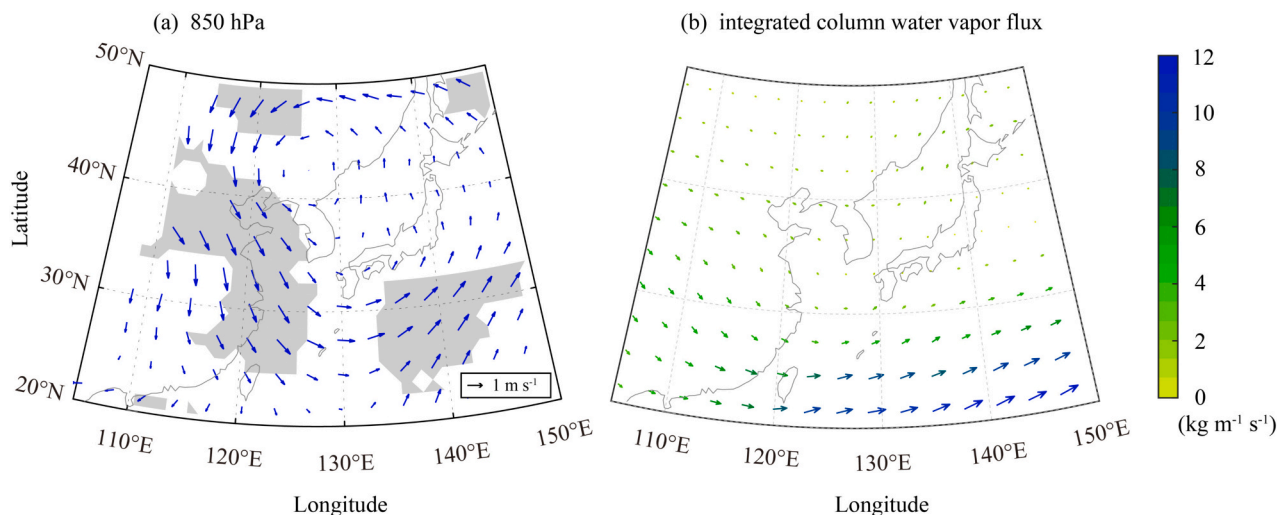


Fig. 5. Spatial pattern of the wind vector anomaly at the 850 hPa pressure level for the five megadroughts (a) and integrated column water vapor flux anomaly (b). Gray shading denotes significance at a confidence level of 0.05.

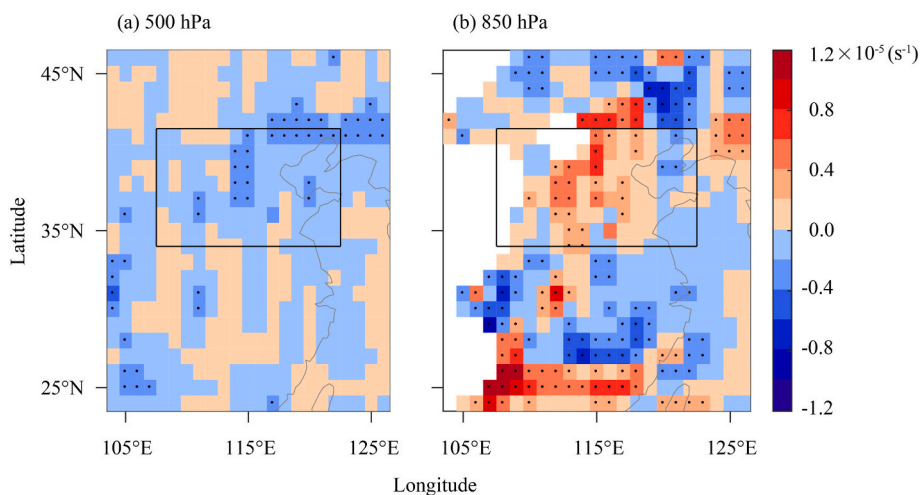


Fig. 6. Spatial pattern of divergence anomaly of the 500 hPa pressure level for the five megadroughts (a) and 850 hPa pressure level (b). The black dots denote significance at a confidence level of 0.05, and the rectangle denotes North China (divergence <0 denotes wind convergence, and divergence >0 denotes wind divergence).

low-pressure centers almost coincided with the climatology European trough and North American trough. Therefore, northerlies in the post-trough pattern over the abovementioned areas may bring little water vapor from high-latitude continents or polar areas, which may lead to precipitation deficits. Taken together, all of the above findings suggest that the eastward wave train induced by the negative NAO deepened the trough and hence formed extensive decadal dry over the NH.

The abovementioned results demonstrated that inconsistent global air temperature cooling, which was affected by external forcing, may decrease the sea level pressure difference by weakening the land-sea thermal contrast. Furthermore, strong northerlies from boreal areas occurred in East China. Combined with vertical downward movement, these factors were unfavorable to precipitation in NC. Meanwhile, the occurrence of a negative NAO triggered by external forcing strengthened the meridional disturbance of Rossby waves in mid-latitudes and deepened troughs in eastern Europe and eastern North America. Northerlies in the post trough region may transport little water vapor, which may lead to extensive decadal drying over the NH.

4. Discussions

4.1. Proxy data-based spatial pattern of hydroclimate accompanied by external forcing

The abovementioned results show that megadroughts in NC and simultaneous decadal dry conditions over the NH may be caused by external forcing, i.e., anomalous solar irradiation and volcanic eruptions in the preindustrial period. Furthermore, we discussed the proxy data-based spatial pattern of hydroclimate in the context of large volcanoes or solar irradiation minimum periods. In detail, following the volcanic chronology of Gao et al. (2008), we selected large volcano with a volcanic explosivity index (VEI) higher than 4. We also selected five solar irradiation minimum periods, which were 1046–1055, 1320–1329, 1451–1460, 1675–1684, and 1806–1815, by Vieira and Solanki (2010). Fig. 8a shows that decadal dry conditions occurred over most of the NH in the next decade after a large volcanic eruption. Dry conditions extensively occurred in NC, north-central Europe and the eastern US, with dry-wet indices as low as -0.3 . Decadal wet conditions occurred in the southwestern US. This spatial pattern of hydroclimate over the NH

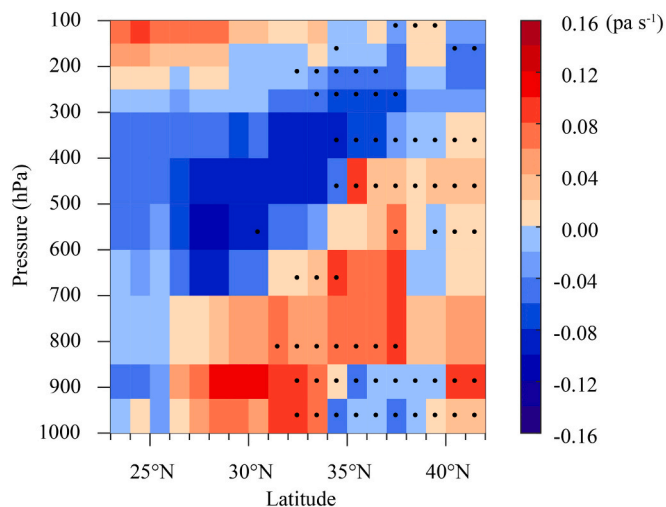


Fig. 7. Vertical average wind anomaly of 105°E-122°E for the five megadroughts. The black dots denote significance at a confidence level of 0.05 ($\sigma < 0$ denotes upward and $\sigma > 0$ denotes downward).

had a high resemblance to that when the five megadroughts occurred. However, Fig. 8b shows wet conditions in NC and weakly dry conditions in the southwestern US compared with Fig. 8a, which was different from

the abovementioned spatial pattern of hydroclimate when megadroughts occurred. This finding indicates that larger volcanic eruptions may play a crucial role in triggering megadroughts in NC and its simultaneous decadal dry conditions over the NH.

Many studies have also reported the climatic effects of volcanic eruptions. For instance, Zheng et al. (2018) reported that the probability of severe drought in East China increased within two years after large volcanic eruptions. Some simulation results show that the decreased incoming solar irradiation at the surface due to volcanic aerosols may weaken the land-ocean thermal gradient and lead to a weakened EASM and less precipitation (Driscoll et al., 2012; Timmreck, 2012; Liu et al., 2016). In addition, Ning et al. (2020) reported that the severest megadroughts of NC in the Ming Dynasty were caused by volcanic eruptions superposing internal variability and were not the impacts of internal variability alone.

4.2. Probability of megadroughts over NC in RCP scenarios

Fig. 9 shows that the precipitation may increase significantly over NC under the RCP scenarios but with the exception of RCP4.5 of the BCC-CSM1.1 model. The IPCC (2013) reported that global temperature would increase by 1.85 °C and 3.7 °C to the end of the 21st century under the RCP4.5 and RCP8.5 scenarios, respectively. Following the Clausius-Clapeyron rules that water vapor content increases 7% with 1 °C warming, climate warming is thereby favorable for precipitation (Liu et al., 2020). Hence, the increased precipitation in the context of climate

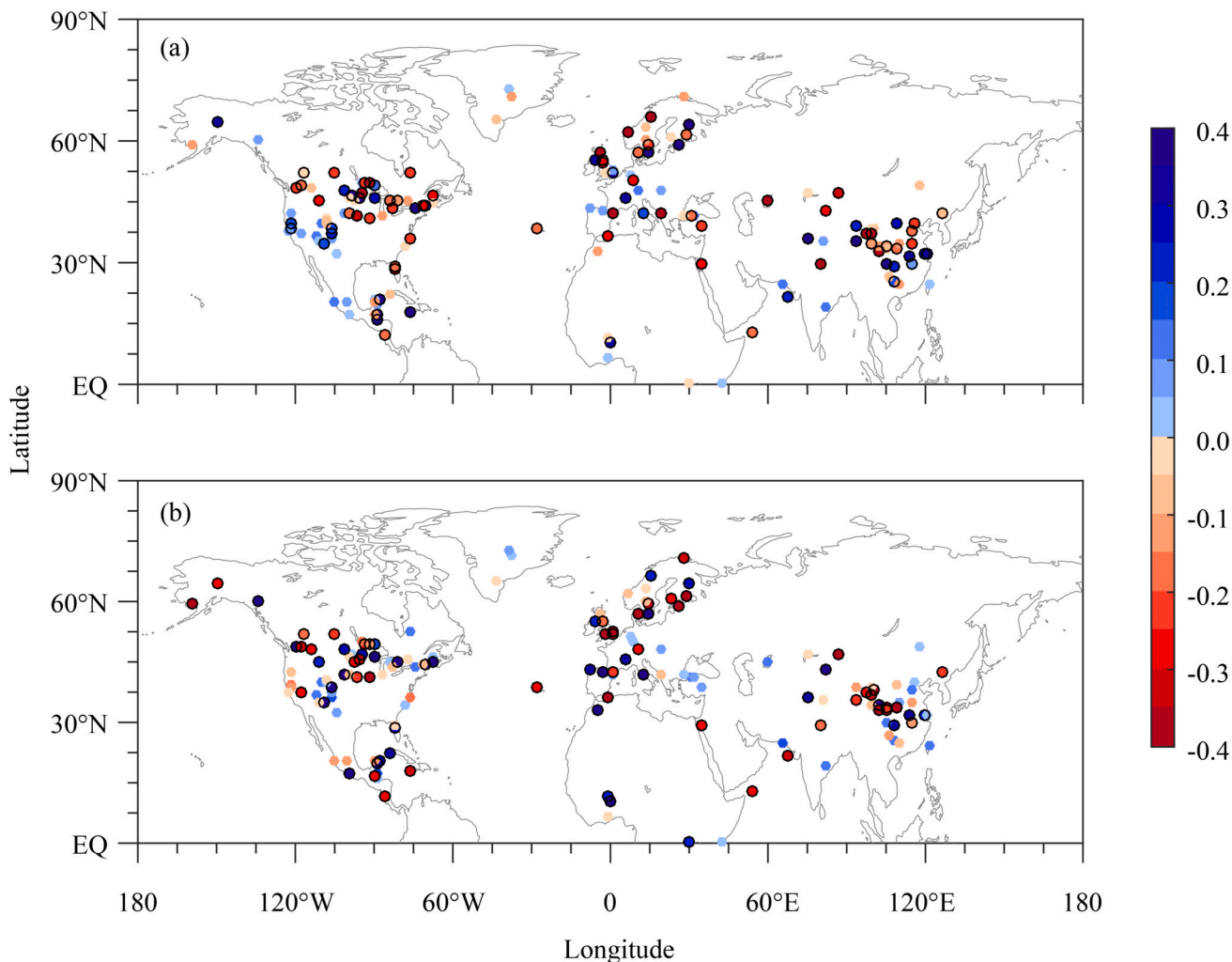


Fig. 8. Spatial pattern of hydroclimate over the NH following large volcanic eruptions (a) and solar irradiation minimum period (b) during the preindustrial period. The black dots denote significance at a confidence level of 0.05.

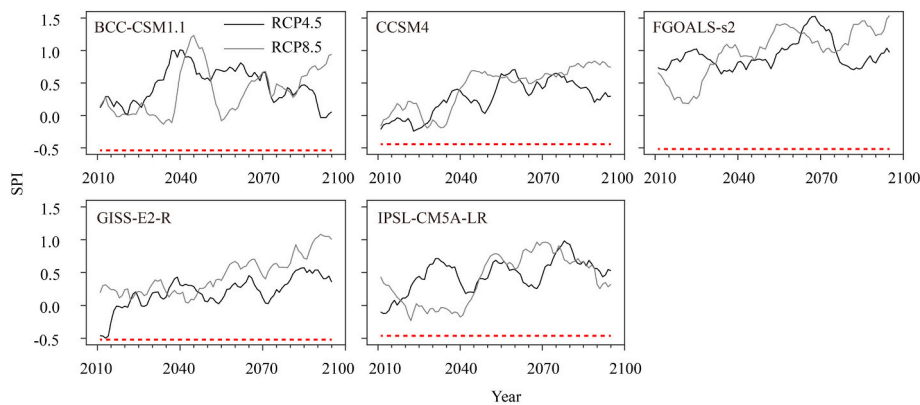


Fig. 9. SPI variations (relative to 850–1850 CE) of NC under two RCP scenarios. The red dotted line represents the criterion of the fifth megadrought of NC during the preindustrial period in each model. (For interpretation of the references to colour in this figure legend, the reader is referred to the web version of this article.)

warming is reasonable. However, it is noted that precipitation increments under the RCP scenarios from different models were inconsistent with each other. For instance, the slope of SPI in FGOALS-s2 are much lower than the slope in CCSM4. So, the sensitivities of precipitation to global warming are different among these climate models. Meanwhile, the dominant temporal scales of SPI oscillations after detrending are also different from one climate model to another. For instance, in the FGOALS-s2, the decadal scale is dominant for the detrended SPI variations under RCP8.5 and the multi-decadal scale is dominant under RCP4.5; however, in the IPSL-CM5A-LR, it is reversely. These discrepancies are mainly caused by model uncertainties, which are mostly derived from the models' dynamic frame and physical parameterizations. Because of the model discrepancies, the multiple model ensemble mean approach is extensively applied. The multiple model ensemble mean may diminish the bias of models caused by model uncertainties, which is also the main reason why we used the results of five models rather than individual models.

By comparing the precipitation prediction provided by the climate models to the megadrought criteria, we found that megadrought-like events would not reoccur under the RCP scenarios (Fig. 9). However, this illustration may be impossible because the predicted precipitation may be overestimated. Following the experimental design of CMIP5 for future climate prediction under the RCP scenarios, these climate models only considered the anthropogenic emissions of greenhouse gas rather than the natural external forcing, such as large volcanic eruptions and abnormal solar irradiation. Our abovementioned results demonstrate that abnormal external forcing together with internal variability may lead to megadroughts. Therefore, climate prediction in the absence of abnormal external forcing may overestimate the prediction. Therefore, the illustration that future precipitation remains higher than the megadrought criteria may not be reliable. Depending on this result, we suggest that it may be valuable to consider abnormal natural external forcing (e.g., volcanic eruptions) in future climate predictions to improve megadrought predictions.

5. Conclusions

The abovementioned results demonstrated that in full forcing simulations, megadroughts in NC were generally accompanied by extensive decadal drying over the NH, especially over most of North America and Europe. This spatial pattern of hydroclimate remains consistent with that in the proxy data; however, it could not be reproduced by the control simulations forced only by internal variability. These findings suggest that megadroughts in NC and simultaneous extensive decadal dry conditions over the NH could not occur in the absence of abnormal natural external forcing, such as large volcanic eruptions.

The anomalous natural external forcing may lead to global cooling. Moreover, climate cooling may lead to atmospheric water vapor decline, which is unfavorable for precipitation in NC. In the context of climate

cooling, the land-sea thermal contrast weakened; hence, the zonal pressure gradient from the West Pacific to East Asia was weakened. As a result, the water vapor transport declined and was also unfavorable for precipitation in NC. For the megadrought in NC, the full forcing simulations show that there was generally a negative NAO that formed an eastward wave train in the mid-latitudes, which intensified meridional disturbance of the Rossby wave. Northerlies in the post-trough pattern over Europe and North America may bring little water vapor from high-latitude continents or Arctic areas. Consequently, extensive decadal drying occurred over the NH.

This study implies that extensive decadal dry conditions may occur over the NH. Since there are many populations and economies in East Asia, Europe and North America, such hydroclimate conditions at the decadal scale may decrease the supply capacity of grain over the NH and lead to an economic recession, which would lead to catastrophic damage for the world. To prevent extensive dry risks across multiple continents, we investigated decadal dry conditions from a hemispheric perspective and analyzed the hydroclimatic relationship of other areas with NC.

Meanwhile, using the SPI anomaly to represent hydroclimate may be insufficient since the hydroclimate is determined together by precipitation, evapotranspiration, etc. (Dai, 2011). Notably, neither full forcing experiments nor control experiments could reproduce proxy-based wet conditions in Central Asia. In the context of global cooling conditions affected by external forcing, the proxy illustration characterized by cumulative soil moisture was wetter since there was less evapotranspiration. In contrast, the SPI indicated by using precipitation alone in the models presented dry conditions because of external forcing. Then, we only used one output from each model. The contamination of climate internal variability on research results may not be removed completely with the multi-model ensemble mean method. Large sample ensemble results for one climate model, such as CESM-LME, may represent another method of weakening contamination caused by climate internal variability on the research results. Finally, when discussing the spatial pattern of hydroclimate accompanied by external forcing, it is better to design climate simulation experiments of independent external forcing to further understand the potential causes of the effects of external forcing.

Declaration of competing interest

The authors declare that they have no conflicts of interest.

Acknowledgements

This research was supported by the National Key R&D Program of China on Global Change (Grant nos. 2016YFA0600401, 2017YFA0603301), the Key Research Program of Frontier Sciences from CAS (No. ZDRWZS-2017-4). CMIP5 model outputs were downloaded from <https://esgf-data.dkrz.de/search/cmip5-dkrz/> website.

References

- Bothe, O., Jungclauss, J.H., Zanchettin, D., Zorita, E., 2013. Climate of the last millennium: ensemble consistency of simulations and reconstructions. *Clim. Past* 9 (3), 1089–1110. <https://doi.org/10.5194/cp-9-1089-2013>.
- Chen, F.H., Chen, J.H., Holmes, J., Boomer, I., Austin, P., Gates, J.B., Wang, N., Brooks, S.J., Zhang, J., 2010. Moisture changes over the last millennium in arid Central Asia: a review, synthesis and comparison with monsoon region. *Quat. Sci. Rev.* 29, 1055–1068. <https://doi.org/10.1016/j.quascirev.2010.01.005>.
- Chen, J., Liu, Y.J., Pan, T., Liu, Y.H., Sun, F.B., Ge, Q.S., 2018. Population exposure to droughts in China under the 1.5 degrees C global warming target. *Earth Syst. Dyn.* 9 (3), 1097–1106. <https://doi.org/10.5194/esd-9-1097-2018>.
- Coats, S., Smerdon, J.E., Cook, B.I., Seager, R., Cook, E.R., Anchukaitis, K.J., 2016. Internal Ocean-atmosphere variability drives megadroughts in Western North America. *Geophys. Res. Lett.* 43 (18), 9886–9894. <https://doi.org/10.1002/2016GL070105>.
- Cook, E.R., Anchukaitis, K.J., Buckley, B.M., D'Arrigo, R.D., Jacoby, G.C., Wright, W.E., 2010. Asian Monsoon failure and megadrought during the last millennium. *Science* 328 (5977), 486–489. <https://doi.org/10.1126/science.1185188>.
- Cook, B.I., Cook, E.R., Smerdon, J.E., Seager, R., Williams, A.P., Coast, S., Stahle, D.W., Diaz, J.V., 2016. North American megadroughts in the Common Era: reconstructions and simulations. *WIREs Clim. Chang.* 7 (3), 411–432. <https://doi.org/10.1002/wcc.394>.
- Dai, A.G., 2011. Characteristics and trends in various forms of the Palmer Drought Severity Index during 1900–2008. *J. Geophys. Res. Atmos.* 116 <https://doi.org/10.1029/2010JD015541>.
- Driscoll, S., Bozzo, A., Gray, L.J., Robock, A., Stenchikov, G., 2012. Coupled Model Intercomparison Project 5 (CMIP5) simulations of climate following volcanic eruptions. *J. Geophys. Res. Atmos.* 117, D17105 <https://doi.org/10.1029/2012JD017607>.
- Erling, J.M., Gourley, J.J., Basara, J.B., 2019. Diagnosing moisture sources for flash floods in the United States. Part II: terrestrial and oceanic sources of moisture. *J. Hydrometeorol.* 20 (8), 1511–1531. <https://doi.org/10.1175/JHM-D-18-0120.1>.
- Gao, C.C., Robock, A., Ammann, C., 2008. Volcanic forcing of climate over the past 1500 years: an improved ice core-based index for climate models. *J. Geophys. Res. Atmos.* 113 <https://doi.org/10.1029/2008JD010239>.
- Ge, Q.S., Zheng, J.Y., Hao, Z.X., Liu, H.L., 2013. General characteristics of climate changes during the past 2000 years in China. *Sci. China Earth Sci.* 56 (2), 321–329. <https://doi.org/10.1007/s11430-012-4370-y>.
- Graham, N.E., Ammann, C.M., Fleitmann, D., Cobb, K.M., Luterbacher, J., 2011. Support for global climate reorganization during the “Medieval Climate Anomaly”. *Clim. Dyn.* 37, 1217–1245. <https://doi.org/10.1007/s00382-010-0914-z>.
- Hao, Z.X., Wu, M.W., Zheng, J.Y., Chen, J.W., Zhang, X.Z., Luo, S.W., 2020. Patterns in data of extreme droughts/floods and harvest grades derived from historical documents in eastern China during 801–1910. *Clim. Past* 16 (1), 101–116. <https://doi.org/10.5194/cp-16-101-2020>.
- Henson, S.A., Painter, S.C., Holliday, N.P., Stinchcombe, M.C., Giering, S.L.C., 2013. Unusual subtropical North Atlantic phytoplankton bloom in 2010: Volcanic fertilization or North Atlantic Oscillation? *J. Geophys. Res. Ocean* 118 (10), 4771–4780. <https://doi.org/10.1002/jgrc.20363>.
- IPCC, 2013. *Climate Change 2013: The Physical Science Basis. Contribution of Working Group I to the Fifth Assessment Report of the Intergovernmental Panel on Climate Change.* Cambridge University Press, Cambridge, UK.
- Jiang, S., Wang, J.H., Zhao, Y., Shang, Y.Z., Gao, X.R., Li, H.H., Wang, Q.M., Zhu, Y.N., 2017. Sustainability of water resources for agriculture considering grain production, trade and consumption in China from 2004 to 2013. *J. Clean. Prod.* 149, 1210–1218. <https://doi.org/10.1016/j.jclepro.2017.02.103>.
- Liu, F., Chai, J., Wang, B., Liu, J., Zhang, X., Wang, Z.Y., 2016. Global monsoon precipitation responses to large volcanic eruptions. *Sci. Rep.* 6 <https://doi.org/10.1038/srep24331>.
- Liu, Y.Y., Li, Y., Ding, Y.H., 2020. East Asian summer rainfall projection and uncertainty under a global warming scenario. *Int. J. Climatol.* 40 (11), 4828–4842. <https://doi.org/10.1002/joc.6491>.
- Ljungqvist, F.C., Krusic, P.J., Sundqvist, H.S., Zorita, E., Brattstrom, G., Frank, D., 2016. Northern Hemisphere hydroclimate variability over the past twelve centuries. *Nature* 532, 94–110. <https://doi.org/10.1038/nature17418>.
- Ljungqvist, F.C., Seim, A., Krusic, P.J., Gonzalez-Rouco, J.F., Werner, J.P., Cook, E.R., Zorita, E., Luterbacher, J., Xoplaki, E., Destouni, G., Garcia-Bustainante, E., Aguilar, C.A.M., Seftigen, K., Wang, J.L., Gagen, M.H., Esper, J., Solomina, O., Fleitmann, D., Buntgen, U., 2019. European warm-season temperature and hydroclimate since 850 CE. *Environ. Res. Lett.* 14 (8) <https://doi.org/10.1088/1748-9326/ab2c7e>.
- Man, W.M., Zhou, T.J., Jungclauss, J.H., 2012. Simulation of the East Asian Summer Monsoon during the last millennium with the MPI earth system model. *J. Clim.* 25 (22), 7852–7866. <https://doi.org/10.1175/JCLI-D-11-00462.1>.
- McKee, T.B., Doesken, N.J., Doesken, J., 1993. The relationship of drought frequency and duration to time scale. In: *Proceedings of the Eighth Conference on Applied Climatology.* American Meteorological Society, Anaheim, California, pp. 179–184.
- Ning, L., Chen, K.F., Liu, J., Liu, Z.Y., Yan, M., Sun, W.Y., Jin, C.H., Shi, Z.G., 2020. How do volcanic eruptions influence decadal megadroughts over eastern China? *J. Clim.* <https://doi.org/10.1175/JCLI-D-19-0394.1>.
- Ning, L., Liu, J., Wang, B., Chen, K.F., Yan, M., Jin, C.H., Wang, Q.R., 2019. Variability and mechanisms of megadroughts over Eastern China during the last millennium: a model study. *Atmosphere* 10 (1). <https://doi.org/10.3390/atmos10010007>.
- Ohba, M., Shiogama, H., Yokohata, T., Watanabe, M., 2013. Impact of strong tropical volcanic eruptions on ENSO simulated in a coupled GCM. *J. Clim.* 26 (14), 5169–5182. <https://doi.org/10.1175/JCLI-D-12-00471.1>.
- Peng, Y.B., 2018. Simulated interannual teleconnection between the summer North Atlantic oscillation and summer precipitation in Eastern China during the last millennium. *Geophys. Res. Lett.* 45 (15), 7741–7747. <https://doi.org/10.1029/2018GL078691>.
- Schneider, D.P., Ammann, C.M., Otto-Bliesner, B.L., Kaufman, D.S., 2009. Climate response to large, high-latitude and low-latitude volcanic eruptions in the Community Climate System Model. *J. Geophys. Res. Atmos.* 114, D15101 <https://doi.org/10.1029/2008JD011222>.
- Schneider, L., Ljungqvist, F.C., Yang, B., Chen, F.H., Chen, J.H., Li, J.Y., Hao, Z.X., Ge, Q.S., Talento, S., Osborn, T.J., Luterbacher, J., 2019. The impact of proxy selection strategies on a millennium-long ensemble of hydroclimatic records in Monsoon Asia. *Quat. Sci. Rev.* 223, 105917. <https://doi.org/10.1016/j.quascirev.2019.105917>.
- Shen, C., Wang, W.C., Hao, Z.X., Gong, W., 2007. Exceptional drought events over eastern China during the last five centuries. *Clim. Chang.* 85 (3–4), 453–471. <https://doi.org/10.1007/s10584-007-9283-y>.
- Shi, F., Zhao, S., Guo, Z.T., Goosse, H., Yin, Q.Z., 2017. Multi-proxy reconstructions of May–September precipitation field in China over the past 500 years. *Clim. Past* 13 (12), 1919–1938. <https://doi.org/10.5194/cp-13-1919-2017>.
- Stegehuis, A.L., Vautard, R., Ciais, P., Teuling, A.J., Jung, M., Yiou, P., 2013. Summer temperatures in Europe and land heat fluxes in observation-based data and regional climate model simulations. *Clim. Dyn.* 41 (2), 455–477. <https://doi.org/10.1007/s00382-012-1559-x>.
- Stevenson, S., Otto-Bliesner, B., Fasullo, J., Brady, E., 2016. “El Nino Like” hydroclimate responses to last millennium volcanic eruptions. *J. Clim.* 29 (8), 2907–2921. <https://doi.org/10.1175/JCLI-D-15-0239.1>.
- Sun, W.Y., Wang, B., Liu, J., Chen, D.L., Gao, C.C., Ning, L., Chen, L., 2019. How northern high-latitude volcanic eruptions in different seasons affect ENSO. *J. Clim.* 32 (11), 3245–3262. <https://doi.org/10.1175/JCLI-D-18-0290.1>.
- Taylor, K.E., Stouffer, R.J., Meehl, G.A., 2012. An overview of CMIP5 and the experiment design. *Bull. Am. Meteorol. Soc.* 93, 485–498. <https://doi.org/10.1175/BAMS-D-11-00094.1>.
- Timmreck, C., 2012. Modeling the climatic effects of large explosive volcanic eruptions. *WIREs Clim. Chang.* 3 (6), 545–564. <https://doi.org/10.1002/wcc.192>.
- van Loon, H., Meehl, G.A., Shea, D.J., 2007. Coupled air-sea response to solar forcing in the Pacific region during northern winter. *J. Geophys. Res. Atmos.* 112 (D2), D02108 <https://doi.org/10.1029/2006JD007378>.
- Vieira, L.E.A., Solanki, S.K., 2010. Evolution of the solar magnetic flux on time scales of years to millennia. *Astron. Astrophys.* 509 <https://doi.org/10.1051/0004-6361/200913276>.
- Wang, A.H., Lettenmaier, D.P., Sheffield, J., 2011. Soil Moisture Drought in China, 1950–2006. *J. Clim.* 24 (13), 3257–3271. <https://doi.org/10.1175/2011JCLI3733.1>.
- Wang, J.Y., Zhang, Z.W., Liu, Y.S., 2018. Spatial shifts in grain production increases in China and implications for food security. *Land Use Policy* 74, 204–213. <https://doi.org/10.1016/j.landusepol.2017.11.037>.
- Xie, N.M., Xin, J.H., Liu, S.F., 2014. China's regional meteorological disaster loss analysis and evaluation based on grey cluster model. *Nat. Hazards* 71 (2), 1067–1089. <https://doi.org/10.1007/s11069-013-0662-6>.
- Yang, Q., Ma, Z.G., Fan, X.G., Yang, Z.L., Xu, Z.F., Wu, P.L., 2017. Decadal modulation of precipitation patterns over Eastern China by sea surface temperature anomalies. *J. Clim.* 30 (17), 7017–7033. <https://doi.org/10.1175/JCLI-D-16-0793.1>.
- Yang, Q., Ma, Z.G., Wu, P.L., Klingaman, N.P., Zhang, L.X., 2019. Interdecadal seesaw of precipitation variability between North China and the Southwest United States. *J. Clim.* 32(10), 2951–2968. *J. Clim.* 32 (10), 2951–2968. <https://doi.org/10.1175/JCLI-D-18-0082.1>.
- Yu, M.X., Li, Q.F., Hayes, M.J., Svoboda, M.D., Heim, R.R., 2014. Are droughts becoming more frequent or severe in China based on the standardized precipitation evapotranspiration index: 1951–2010? *Int. J. Climatol.* 34 (3), 545–558. <https://doi.org/10.1002/joc.3701>.
- Yuan, X., Wang, L.Y., Wu, P.L., Ji, P., Sheffield, J., Zhang, M., 2019. Anthropogenic shift towards higher risk of flash drought over China. *Nat. Commun.* 10, 4661. <https://doi.org/10.1038/s41467-019-12692-7>.
- Zarei, A.R., Moghimi, M.M., Mahmoudi, M.R., 2016. Analysis of changes in spatial pattern of drought using RDI index in south of Iran. *Water Resour. Manag.* 30 (11), 3723–3743. <https://doi.org/10.1007/s11269-016-1380-0>.
- Zheng, J.Y., Wang, W.C., Ge, Q.S., Man, Z.M., Zhang, P.Y., 2006. Precipitation variability and extreme events in eastern China during the past 1500 years. *Terr. Atmos. Ocean. Sci.* 17 (3), 579–592.
- Zheng, J.Y., Xiao, L.B., Fang, X.Q., Hao, Z.X., Ge, Q.S., Li, B.B., 2014. How climate change impacted the collapse of the Ming dynasty. *Clim. Chang.* 127, 169–182. <https://doi.org/10.1007/s10584-014-1244-7>.
- Zheng, J.Y., Yu, Y.Z., Zhang, X.Z., Hao, Z.X., 2018. Variation of extreme drought and flood in North China revealed by document-based seasonal precipitation reconstruction for the past 300 years. *Clim. Past* 14 (8), 1135–1145. <https://doi.org/10.5194/cp-14-1135-2018>.
- Zhou, X.C., Jiang, D.B., Lang, X.M., 2020. Unstable relationship between the Pacific Decadal Oscillation and eastern China summer precipitation: insights from the Medieval Climate Anomaly and Little Ice Age. *Holocene* 30 (6), 799–809. <https://doi.org/10.1177/0959683620902215>.